

# A theoretical analysis of the effects of electron-withdrawing substitutions on electronic structures and phosphorescent efficiency of a series of Ir(III) complexes with 2-phenylpyridine ligands

Xue-Feng Ren<sup>1</sup> · Guo-Jun Kang<sup>1,2</sup> · Qiong-Qiong He<sup>1</sup> · Chuan-Yue Zheng<sup>1,2</sup> · Xiang-Kun Ren<sup>1,2</sup>

Received: 25 August 2015 / Accepted: 30 November 2015 / Published online: 5 January 2016  
© Springer-Verlag Berlin Heidelberg 2016

**Abstract** A density functional theory and time-dependent density functional theory approaches were used to understand the structure–property relationships of a series of Ir(III) complexes  $\text{Ir}(x\text{-NHC})(y\text{-ppy})_2$  [where NHC = 2,3-dihydro-1-methyl-3-phenyl-1H-imidazole, ppy = 2-phenylpyridine,  $x = \text{Cl}$ ,  $y = \text{H}$  (**1a**);  $x = \text{Cl}$ ,  $y = \text{Cl}$  (**1a-Cl**);  $x = \text{Cl}$ ,  $y = \text{F}$  (**1a-F**);  $x = \text{Cl}$ ,  $y = \text{CN}$  (**1a-CN**);  $x = \text{Cl}$ ,  $y = \text{CF}_3$  (**1a-CF<sub>3</sub>**);  $x = \text{F}$ ,  $y = \text{CF}_3$  (**2-CF<sub>3</sub>**)]. The investigations on the electronic structures in the ground and lowest triplet excited states, the frontier molecular orbitals, the absorption and emission spectra, as well as charge injection and transport of these Ir complexes provided a good understanding of the structure–property relationships. Furthermore, the full details of the metal character in the phosphorescent spectra (<sup>3</sup>MLCT %), triplet energy ( $E_{\text{T}_1}$ ), the singlet–triplet splitting energy ( $\Delta E_{\text{S}_1\text{-T}_1}$ ), <sup>3</sup>MLCT–<sup>3</sup>MC energy gap, as well as d orbitals splitting revealed that quantum yield was effectively enhanced by introducing CN and CF<sub>3</sub> groups on the ppy ligands. The

designed complexes **1-CN**, **1-CF<sub>3</sub>**, and **2-CF<sub>3</sub>** are expected to be highly efficient phosphorescent materials in organic light-emitting diodes.

**Keywords** Iridium complexes · Density functional theory · 2-Phenylpyridine

## 1 Introduction

Phosphorescent iridium(III) complexes have attracted considerable attention for their greatly potential application as highly efficient electroluminescent (EL) emitters in organic light-emitting diodes (OLEDs) [1–3]. Greater success has been achieved in developing the Ir(III) type emitters with 2-phenylpyridine (ppy) ligand [4–6]. For example, the green light emitting tris(2-phenylpyridine) iridium [Ir(ppy)<sub>3</sub>] exhibits very bright phosphorescence with 90 % efficiency and fast charge injection and transport, which makes Ir(ppy)<sub>3</sub> highly attractive for application in OLEDs [4, 7, 8]. In order to meet the requirements of red–green–blue (RGB) full-color displays, enormous efforts have been devoted to modifying the chemical structure of cyclometalated ligands [9–14].

Most recently, String et al. [15] synthesized a series of blue emitters with two ppy groups in combination with N-heterocyclic carbenes (NHC) unit. It was found that the introduction of the electron-withdrawing (Cl, F) and electron-donating (OMe) groups in the NHC ligand exerted a great influence on the photoluminescence properties. Although the previous study [16] has qualitatively analyzed the effect of F atoms on the metal-to-ligand charge transfer (MLCT) and radiative decay rate ( $k_r$ ), detailed analyses about the nonradiative decay rate ( $k_{nr}$ ),

**Electronic supplementary material** The online version of this article (doi:10.1007/s00214-015-1773-9) contains supplementary material, which is available to authorized users.

✉ Guo-Jun Kang  
gjkang@cumt.edu.cn

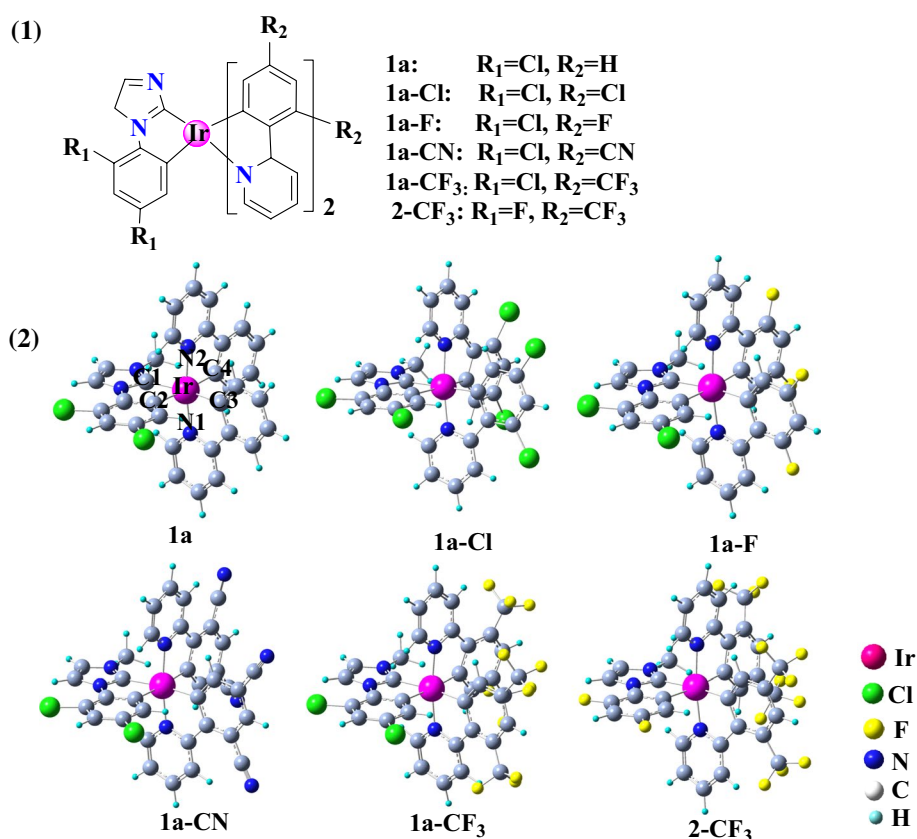
✉ Xiang-Kun Ren  
renxiangkun@baojukeji.com

Xue-Feng Ren  
renxf@cumt.edu.cn

<sup>1</sup> School of Chemical Engineering and Technology, China University of Mining and Technology, Xuzhou 221008, China

<sup>2</sup> Low Carbon Energy Institute, China University of Mining and Technology, Xuzhou 221008, China

**Fig. 1** The (1) schematic structures and (2) optimized ground state geometry of studied Ir complexes



to the methodology suggested in Thummel's work [23]. For a better analysis of the nature of the excited states involved in the emission process, natural orbital transition (NTO) analyses [24] were performed via TD-DFT approach. All the calculations were made with the Gaussian09 software package [25].

### 3 Results and discussion

#### 3.1 Geometries in ground and lowest-lying triplet excited states

The schematic structures and optimized ground state geometries of six complexes are shown in Fig. 1, together with the number of some key atoms. The metal–ligand bond lengths and bond angles of investigated complexes are collected in Table 1.

Table 1 shows that the changes of these bond angles are minor from complex **1a** to these designed materials. As

shown in Fig. 1, all these studied complexes adopt a distorted octahedral geometry, which are caused by the  $d^6$  configuration of the Ir(III) center. Besides, the calculated results show that the Ir–C1 (2.075 Å) and Ir–C2 (2.111 Å) bond lengths in complex **1a** are shortened by 0.012 and 0.005 Å, respectively, in comparison with those of F-substituted NHC complex **1** (2.087 Å for Ir–C1 and 2.116 Å for Ir–C2) [16]. Clearly, the Cl substitutions in NHC moiety have great influence on the metal–ligand relative to F substitutions, which will increase the probability of charge transfer from the metal to the ligand. In addition, the calculated metal–ligand bond lengths Ir–C3, Ir–C4, Ir–N1, and Ir–N2 on ppy ligands of complex **1a** are much shorter than those on NHC ligand (Ir–C1 and Ir–C2 bond lengths), suggesting a strong interaction between Ir metal center and the ppy ligands. Therefore, the introduction of the F, Cl, CN, and CF<sub>3</sub> substitutions on the ppy ligands could be efficient strategies to tune the geometry and photophysical properties. As collected in Table 1, the Ir–C3, Ir–N1, Ir–C4, Ir–N2 bonds for **1a-Cl** (2.038, 2.048, 2.056, and 2.054 Å,

**Table 1** The selected key bond lengths (Å) and bond angles (°) for studied complexes in the ground (S0) and lowest-lying triplet state (T1) geometry

|                 | <b>1a</b>    |       | <b>1a-Cl</b>             |       | <b>1a-F</b>             |       |
|-----------------|--------------|-------|--------------------------|-------|-------------------------|-------|
|                 | S0           | T1    | S0                       | T1    | S0                      | T1    |
| Bond length (Å) |              |       |                          |       |                         |       |
| Ir-C1           | 2.075        | 2.073 | 2.076                    | 2.064 | 2.074                   | 2.062 |
| Ir-C2           | 2.111        | 2.108 | 2.111                    | 2.104 | 2.110                   | 2.103 |
| Ir-C3           | 2.043        | 2.043 | 2.038                    | 2.042 | 2.039                   | 2.046 |
| Ir-N1           | 2.055        | 2.051 | 2.048                    | 2.003 | 2.056                   | 2.004 |
| Ir-C4           | 2.063        | 2.049 | 2.056                    | 2.058 | 2.059                   | 2.061 |
| Ir-N2           | 2.062        | 2.030 | 2.054                    | 2.056 | 2.060                   | 2.064 |
| Bond angle (°)  |              |       |                          |       |                         |       |
| C1-Ir-C2        | 77.1         | 77.7  | 77.1                     | 77.9  | 77.1                    | 77.9  |
| C1-Ir-C4        | 101.0        | 99.6  | 100.7                    | 102.2 | 100.9                   | 102.2 |
| C3-Ir-N1        | 79.7         | 80.1  | 79.2                     | 81.2  | 79.8                    | 81.6  |
| N2-Ir-N1        | 171.7        | 172.2 | 171.7                    | 172.2 | 171.6                   | 172.3 |
|                 | <b>1a-CN</b> |       | <b>1a-CF<sub>3</sub></b> |       | <b>2-CF<sub>3</sub></b> |       |
|                 | S0           | T1    | S0                       | T1    | S0                      | T1    |
| Bond length (Å) |              |       |                          |       |                         |       |
| Ir-C1           | 2.079        | 2.073 | 2.077                    | 2.090 | 2.094                   | 2.087 |
| Ir-C2           | 2.110        | 2.112 | 2.114                    | 2.123 | 2.114                   | 2.122 |
| Ir-C3           | 2.038        | 2.040 | 2.033                    | 2.029 | 2.032                   | 2.033 |
| Ir-N1           | 2.051        | 2.046 | 2.047                    | 2.044 | 2.045                   | 2.039 |
| Ir-C4           | 2.057        | 2.035 | 2.057                    | 2.012 | 2.052                   | 2.016 |
| Ir-N2           | 2.057        | 2.034 | 2.055                    | 2.041 | 2.055                   | 2.042 |
| Bond angle (°)  |              |       |                          |       |                         |       |
| C1-Ir-C2        | 77.1         | 77.6  | 77.0                     | 77.0  | 77.7                    | 78.0  |
| C1-Ir-C4        | 100.9        | 99.8  | 101.9                    | 97.2  | 98.0                    | 98.8  |
| C3-Ir-N1        | 79.2         | 79.7  | 79.0                     | 79.6  | 78.9                    | 79.3  |
| N2-Ir-N1        | 171.8        | 172.4 | 171.6                    | 173.1 | 172.2                   | 172.8 |

respectively) are much shortened compared to those for **1a** (2.043, 2.055, 2.063, and 2.062 Å, respectively). This means that the interactions between the metal and ppy ligands are strengthened by importing the Cl atoms. Similar shortening for the Ir–C and Ir–N bonds (by ca. 0.01 Å) also observed for **1a-F**, **1a-CN**, **1a-CF<sub>3</sub>**, and **2-CF<sub>3</sub>**. Normally, the strengthened metal–ligand bond may increase the probability of charge transfer from the metal center to ppy ligands, which will be further testified in the following section.

In order to gain insight into the geometric relaxations upon excitation, the geometries parameters at the lowest-lying triplet excited states (T1) of studied complexes are also collected in Table 1. As listed in Table 1, all the metal–ligand bond lengths of complex **1a** at the T1 state are pulled closed to the metal compared with S0 state, especially the bond lengths of Ir–C4 and Ir–N2, which are shortened by 0.014 and 0.032 Å, respectively, upon excitation to T1 state. The strengthened metal–ligand bond is useful to increase the charge transfer from the metal to ligand (MLCT). Furthermore, the Ir–N1 for **1a-Cl** and **1a-F** is contracted by 0.045 and 0.052 Å, respectively, upon S0–T1 excitation. The slightly elongated Ir–C3 for **1a-Cl** and **1a-F** can be easily rationalized by the stronger Ir–N1 bond interaction, which weakened the Ir–C3 at its trans disposition. Similarly, for **1a-CN**, **1a-CF<sub>3</sub>**, and **2-CF<sub>3</sub>**, the Ir–C4 in the T1 state is significantly shortened (0.022, 0.045, and 0.036 Å for **1a-CN**, **1a-CF<sub>3</sub>**, **2-CF<sub>3</sub>**, respectively) compared to the S0 state. Therefore, it can be concluded that the ppy ligand is pulled in closer to the metal by introducing these substitutions, which may facilitate the metal center to ppy ligand charge transfer, eventually improving the phosphorescence quantum efficiency.

### 3.2 Frontier molecular orbitals

To reveal the photophysical properties of these complexes, we will discuss in detail the frontier molecular orbital (FMO) energy levels and components. The main FMO energy level and the contour plots of the HOMO and LUMO are drawn in Fig. 2. The details of FMO compositions of studied complexes are shown in Table S1–S6 in Supporting Information.

Figure 2 shows the HOMO (–5.27 eV) and LUMO (–1.19 eV) values of complex **1a** with Cl substitutions at NHC ligand are much lower than the experimental synthesized complex with no substitutions at NHC ligand (HOMO = –5.02 eV and LUMO = –1.00 eV for **1** [16]) and with F substitutions at NHC ligand (HOMO = –5.17 eV and LUMO = –1.12 eV for **1'** [16]). We also noticed that the **1a-CF<sub>3</sub>** has decreased LUMO (–2.02 eV) energy level compared with that of **2-CF<sub>3</sub>** (–1.97 eV). It is obvious that a type of attracting electron

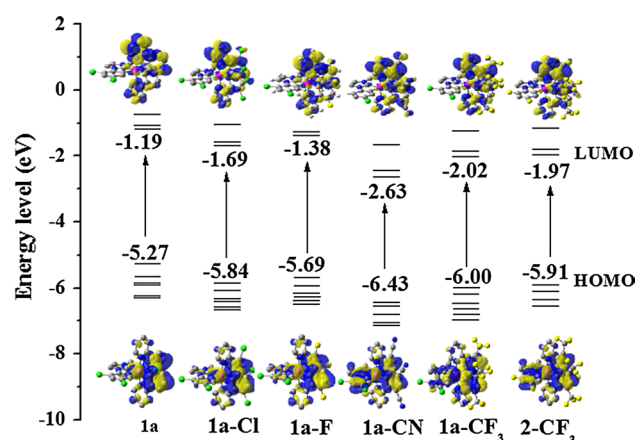


**Fig. 2** The orbital energy level (eV), energy gap (eV), and contour plot of the HOMO and LUMO for studied complexes

transporting materials can be obtained by introducing the Cl atoms on NHC ligand instead of F atoms. In addition, both of HOMO and LUMO energy levels of these Ir complexes are dramatically stabilized by introducing the electron-withdrawing substitutions on ppy ligand compared to applying them on the NHC ligand, which agrees with our previous report [16]. For example, for **1a-F** and **1a-Cl**, the LUMO energy levels are decreased by 0.19 and 0.50 eV, respectively, compared with complex **1a**. This means that the electron injection ability can be effectively tuned by introducing F and Cl atoms at ppy ligands. Moreover, the LUMO energy of **1a-CN**, **1a-CF<sub>3</sub>**, and **2-CF<sub>3</sub>** are dramatically decreased by 1.44, 0.83, 0.78 eV, respectively, compared with that of complex **1a**, which may be attributed to extended conjugated plane (see Fig. 2) between the ppy and NHC in **1a-CN**, **1a-CF<sub>3</sub>**, and **2-CF<sub>3</sub>**. Because of the different degree of decrease in the HOMO and LUMO energy level, the HOMO–LUMO energy gap is decreased in the following order: **1a-F** (4.31 eV) > **1a-Cl** (4.15 eV) > **1a** (4.08 eV) > **1a-CF<sub>3</sub>** (3.98 eV) > **2-CF<sub>3</sub>** (3.94 eV) > **1a-CN** (3.80 eV). It is worth noting that the small HOMO–LUMO gaps of **1a-CF<sub>3</sub>**, **2-CF<sub>3</sub>**, and **1a-CN** might render a red-shift in the emission spectra compared with **1a**. Besides the HOMO and LUMO energy, we also notice that inner molecular orbital energies have been increased relative to their corresponding HOMO levels. The energy gap between HOMO-1 and HOMO is calculated to be 0.24, 0.25, 0.12, 0.19 eV for **1a-Cl**, **1a-F**, **1a-CN**, **1a-CF<sub>3</sub>**, respectively, which is much smaller than those of **1a** (0.39 eV) and **2-CF<sub>3</sub>** (0.79 eV). This indicates that the probabilities of electron transition from inner occupied MOs are increased.

As shown in Fig. 2 and Table S1–S6, all these Ir complexes have similar HOMO and LUMO distribution, i.e., the HOMO is composed of ca. 40 % *d*(Ir), while LUMO is predominantly localized on the  $\pi^*$ (ppy) ligands. But

the contributions from the ligands in these orbitals are different. For example, the HOMO of complex **1a**, **1a-F**, and **1a-Cl** is mainly composed of ca. 55 % $\pi^*$ (ppy), while for **1a-CN**, **1a-CF<sub>3</sub>**, and **2-CF<sub>3</sub>**, their HOMOs are contributed by 25 % $\pi^*$ (Cl-NHC) + 33 % $\pi^*$ (CN-ppy), 9 % $\pi^*$ (Cl-NHC) + 48 % $\pi^*$ (CF<sub>3</sub>-ppy), 20 % $\pi^*$ (F-NHC) + 43 % $\pi^*$ (CF<sub>3</sub>-ppy), respectively. Therefore, the well-conjugated ligands in **1a-CN**, **1a-CF<sub>3</sub>**, and **2-CF<sub>3</sub>** are useful for leading to better electron delocalization over the whole molecule. This would be helpful to understand the trend of the decreased orbital energy levels. In addition, it is also noticed that the contribution of Ir(*d*) to the occupied frontier orbitals are different by adding the substitutions on ppy ligands (see Table S1–S6), all these different distributions will result in different electronic transition characters upon excitation, which will be further discussed in following section.

### 3.3 Absorption spectra

On the basis of the optimized ground state geometry, TD-mPW1PW91 method was used to calculate the absorption properties of these Ir complexes. The simulated absorption spectra for these complexes are presented in Fig. 3. The calculated absorption properties including the absorption wavelength spectra, excitation energies, oscillator strength, main configurations, as well as assignment are collected in Table S7–S12. As depicted in Fig. 3, complex **1a** displays intense high-energy absorption band (230–300 nm) and weaker band in the region of 300–350 nm, which can reproduce the experimental data [15]. Furthermore, the calculated main absorption peaks of complex **1a** are at 394.5, 334.5, 268.5, 256.0, and 237.4 nm (see Table S7), which are well consistent with the experimental values 401, 368, 273, 244, and 215 nm [15], respectively. Thus, the calculations obtained by TD-mPW1PW91 method are

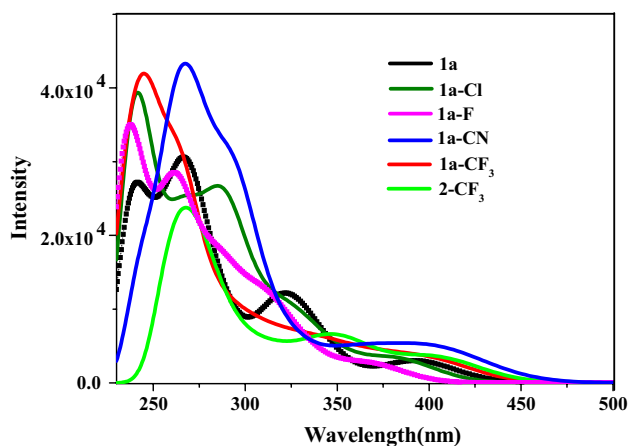


**Fig. 3** Simulated absorption spectra of studied complexes

reliable in understanding the electronic transition of studied complexes.

In order to analyze the nature of absorption, the hole and electron distributions are calculated by Multiwfn software [21]. The hole and electron distributions for the main absorption peaks of **1a** are drawn in Fig. 4, while the hole and electron distributions for other complexes are given in Figure S1 in supporting information. Figure 4 reveals that the S0–S1 and S0–S32 transitions for **1a** mostly process metal-to-ligand charge transfer (MLCT)/intra-ligand charge transfer (ILCT) transition. Because the holes of S1 and S32 states are mainly contributed by Ir(III) atom and ppy moiety, while the electrons are only localized on ppy moiety. For S0–S5, S0–S26, S0–S47 transitions of **1a**, the distribution of their holes is focused on Ir(III) atom, NHC, and ppy moiety, while the electrons are localized on ppy ligands (except for S47 state, the electrons are localized on NHC ligand), and as a result the mixed MLCT/LLCT/ILCT transition occur. According to the orbital component analysis, the differences in the contributions of the Ir(III) atom on hole and electron distribution ( $\Delta$ Ir) dramatically decrease for S26 (18.7 %), S32 (13.7 %), S47 (7.3 %) relative to S1 (40.9 %) and S5 (40.9 %) of **1a**. Thus the amount of MLCT of high-lying absorption band (S0–S26, S0–S32, and S0–S47) of **1a** slightly decreases relative to low-lying absorption band (S0–S1 and S0–S5).

As drawn in Fig. 3, the absorption intensity of these designed Ir complexes is larger than **1a** (except for **2-CF<sub>3</sub>**). Therefore, the probability of the intersystem crossing (ISC) from singlet and triplet state may be well tuned by the introduction of these substituent groups at ppy ligands. The calculated lowest-lying absorption band (S1) of **1a-Cl**, **1a-F**, **1a-CN**, **1a-CF<sub>3</sub>**, and **2-CF<sub>3</sub>** are at 385.9, 369.8, 422.0, 405.8, and 409.7 nm, respectively. Compared with that of **1a** (394.5 nm), **1a-Cl** and **1a-F** complexes are blue-shifted (by 8.6 and 25.5 nm, respectively), while **1a-CN**, **1a-CF<sub>3</sub>**, and **2-CF<sub>3</sub>** are red-shifted (by 27.5, 11.3, 15.2 nm, respectively). This is well consistent with the trend of the HOMO–LUMO energy gaps (see Sect. 3.2), because the excitation of HOMO  $\rightarrow$  LUMO is responsible for the lowest-lying absorption peaks. Based on the hole and electron distributions analysis (Figure S1), all the S1 states for these complexes can be characterized as MLCT/ILCT transition. As expect, the amount of  $\Delta$ Ir in the S1 of **1a-Cl** (43.0 %), **1a-F** (42.4 %), **1a-CN** (46.9 %), **2-CF<sub>3</sub>** (45.3 %), and **1a-CF<sub>3</sub>** (45.5 %) are large relative to **1a** (40.9 %), which means the participation of MLCT in the absorption spectra can be well tuned by introduction of the electron-withdrawing substituent at ppy ligands. Besides, Figure S1 also illustrates all the main absorption peaks for the complexes can be characterized as MLCT/ILCT or MLCT/LLCT transitions. Especially, the high-energy absorption peak of **1a-Cl** (268.4 nm), **1a-CN** (256.2 nm), **2-CF<sub>3</sub>** (237.3 nm) has

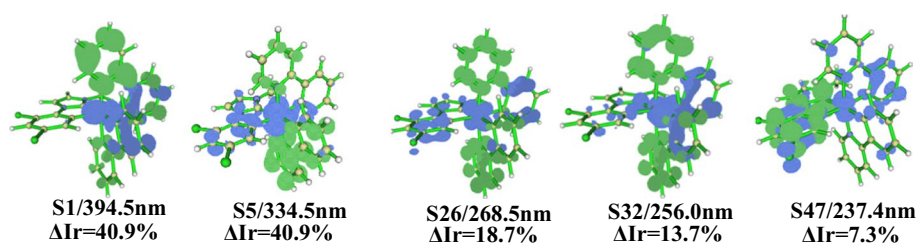


**Fig. 4** The distributions of electron and hole for **1a** at the S1, S5, S26, S32, and S47 state. The *blue* and *green* isosurfaces represent hole and electron distributions, respectively. The differences in the contributions of the Ir(III) atom on hole and electron distribution ( $\Delta Ir$ , %) are collected

**Table 2** The lowest triplet (T1) state for studied complexes calculated by M06-2X method, together with the available experimental values [15]

|                          | Wavelength (nm) | Main configurations        | Assignment   | Exp. [15] |
|--------------------------|-----------------|----------------------------|--|-----------|
| <b>1a</b>                | 496.9           | 0.51 L → H<br>−0.40L → H-1 | $^3MLCT/{}^3ILCT$<br>$^3MLCT/{}^3ILCT/{}^3LLCT$          | 507       |
| <b>1a-Cl</b>             | 495.3           | 0.57 L → H                 | $^3MLCT/{}^3ILCT/{}^3LLCT$                               |           |
| <b>1a-F</b>              | 479.7           | 0.57 L → H                 | $^3MLCT/{}^3ILCT/{}^3LLCT$                               |           |
| <b>1a-CN</b>             | 551.5           | 0.54 L → H<br>0.36 L → H-2 | $^3MLCT/{}^3ILCT/{}^3LLCT$<br>$^3MLCT/{}^3ILCT/{}^3LLCT$ |           |
| <b>1a-CF<sub>3</sub></b> | 538.2           | 0.58 L → H                 | $^3MLCT/{}^3ILCT/{}^3LLCT$                               |           |
| <b>2-CF<sub>3</sub></b>  | 553.2           | 0.59 L → H                 | $^3MLCT/{}^3ILCT/{}^3LLCT$                               |           |

**Table 3** Frontier molecular orbital energies (eV) and compositions (%) of different fragments in the lowest triplet state (T1) for studied complexes

|                          | MO  | Energy (eV) | MO composition  |
|--------------------------|-----|-------------|---|
| <b>1a</b>                | H-1 | −5.86       | 41 %d(Ir) + 26 %π(ppy) + 33 %π(Cl-NHC)                  |
|                          | H   | −5.38       | 39 %d(Ir) + 56 %π(ppy)                                  |
|                          | L   | −1.70       | 96 %π*(ppy)   |
| <b>1a-Cl</b>             | H   | −6.06       | 41 %d(Ir) + 11 %π(Cl-NHC) + 49 %π(Cl-ppy)               |
|                          | L   | −2.24       | 96 %π*(Cl-ppy)  |
| <b>1a-F</b>              | H   | −6.03       | 42 %d(Ir) + 12 %π(Cl-NHC) + 47 %π(F-ppy)                |
|                          | L   | −2.08       | 96 %π*(F-ppy)   |
| <b>1a-CN</b>             | H-2 | −7.01       | 43 %d(Ir) + 36 %π(Cl-NHC) + 21 %π(CN-ppy)               |
|                          | H   | −6.53       | 43 %d(Ir) + 13 %π(Cl-NHC) + 44 %π(CN-ppy)               |
|                          | L   | −3.18       | 97 %π*(CN-ppy)  |
| <b>1a-CF<sub>3</sub></b> | H   | −6.39       | 39 %d(Ir) + 10 %π(Cl-NHC) + 51 %π(CF <sub>3</sub> -ppy) |
|                          | L   | −3.08       | 97 %π*(CF <sub>3</sub> -ppy)                            |
| <b>2-CF<sub>3</sub></b>  | H   | −6.45       | 43 %d(Ir) + 12 %π(F-NHC) + 46 %π(CF <sub>3</sub> -ppy)  |
|                          | L   | −3.08       | 97 %π*(CF <sub>3</sub> -ppy)                            |

35.6, 32.9, and 32.3 %  $\Delta Ir$  contribution, respectively. Obviously, the participation of MLCT in the absorption spectra can be increased by introduction of the Cl, CN, and CF<sub>3</sub>

**Table 4** The integral of overlap of hole-electron (*S*), distance between centroid of hole and electron (*D*, Å), Ir(III) composition to hole (%) and electron (%)

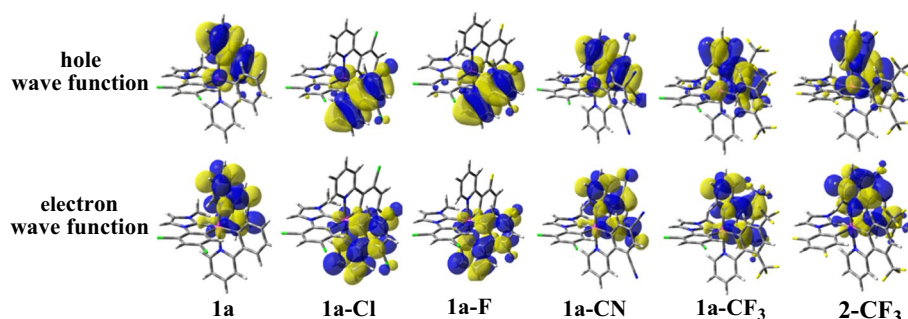
|                          | <i>S</i> | <i>D</i> (Å) | Ir composition to hole (%) | Ir composition to electron (%) |
|--------------------------|----------|--------------|----------------------------|--------------------------------|
| <b>1a</b>                | 0.464    | 1.332        | 16.91                      | 4.74                           |
| <b>1a-Cl</b>             | 0.421    | 1.513        | 16.46                      | 4.68                           |
| <b>1a-F</b>              | 0.370    | 1.519        | 16.65                      | 4.48                           |
| <b>1a-CN</b>             | 0.473    | 0.227        | 17.98                      | 3.82                           |
| <b>1a-CF<sub>3</sub></b> | 0.425    | 0.997        | 27.52                      | 4.40                           |
| <b>2-CF<sub>3</sub></b>  | 0.374    | 0.822        | 23.74                      | 4.40                           |

substituent at ppy ligands. The increased amount of MLCT might be efficient to collect light energy participation of metals and increase the spin-orbital coupling effect. Meanwhile, the intensities of the absorption bands of **1a-Cl**, **1a-CN**, and **1a-CF<sub>3</sub>** are much larger than those of **1a**, which may result in high intensity for the triplet excited states through the ISC procedure, and hence increasing the phosphorescence efficiency.

### 3.4 Phosphorescence properties

As reported in our previous work [16], the TDDFT method with M06-2X functional is reasonable to predict the emission wavelength of this type of compounds. Thus, the M06-2X functional is applied to calculate the emission

**Fig. 5** The hole and electron wave functions of natural transition orbitals (NTO) of Ir complexes for the T1 state



spectra of all the studied molecules. The calculated emission wavelengths, main configurations, as well as assignment are summarized in Table 2, together with the available experimental data [15]. The molecular orbital compositions which are responsible for the emission spectra are summarized in Table 3.

The phosphorescence 496.9 nm of complex **1a** agrees well with the experimental observed value 507 nm, which is contributed by the excitations of HOMO  $\rightarrow$  LUMO and HOMO-1  $\rightarrow$  LUMO. Table 4 shows that the HOMO and HOMO-1 has 39 %Ir(*d*) + 56 % $\pi$ (ppy) and 41 %*d*(Ir) + 26 % $\pi$ (ppy) + 33 % $\pi$ (Cl-NHC), respectively, while LUMO is 96 % $\pi^*$ (ppy) type orbital. Thus, the emission at 496.9 nm can be contributed from 16 %  $^3$ MLCT,  $^3$ LLCT, and  $^3$ ILCT characters. The calculated emission spectra are at 495.3, 479.7, 551.5, 538.2, and 553.2 nm for **1a-Cl**, **1a-F**, **1a-CN**, **1a-CF<sub>3</sub>**, and **2-CF<sub>3</sub>**, respectively. Compared with complex **1a**, the chlorine and fluorine substituted ppy ligand in **1a-Cl** (1.6 nm) and **1a-F** (17.2 nm), respectively, lead to slightly blue shift, which can be easily understood by the widening HOMO–LUMO gap. Combining Tables 3 and 4, the emission of **1a-Cl** and **1a-F** can be described as the  $^3\{d(\text{Ir}) + \pi[(\text{Cl-NHC}) + \text{Cl-ppy}] \rightarrow \pi^*(\text{ppy})\}$  and  $^3\{d(\text{Ir}) + \pi[(\text{Cl-NHC}) + \text{F-ppy}] \rightarrow \pi^*(\text{ppy})\}$  excited state, respectively, which can be described as  $^3$ MLCT/ $^3$ LLCT/ $^3$ ILCT character. For **1a-CN**, **1a-CF<sub>3</sub>**, and **2-CF<sub>3</sub>**, there is a dramatically large red-shifted (by 54.6, 41.3, 56.3 nm, respectively) compared with that of complex **1a**. This indicates that the emitting color of **1a** is efficiently tuned by introducing CF<sub>3</sub> and CN substitutions. As seen from Table 3, the emission of **1a-CN**, **1a-CF<sub>3</sub>**, and **2-CF<sub>3</sub>** at 551.5, 538.2, and 553.2 nm, respectively, is also mainly contributed by LUMO  $\rightarrow$  HOMO transition. Due to the significant composition of the *d*(Ir) orbital in HOMOs, the phosphorescence spectra of **1a-CN**, **1a-CF<sub>3</sub>**, and **2-CF<sub>3</sub>** are mixed characters of  $^3$ MLCT/ $^3$ LLCT/ $^3$ ILCT.

In order to gain a better insight into the nature of the triplet state, the calculated natural transition orbital NTO is depicted in Fig. 5. The NTO eigenvalues ( $\lambda$ ) of these Ir complexes (**1a**: 0.9616; **1a-Cl**: 0.9462; **1a-F**: 0.9413;

**1a-CN**: 0.9766; **1a-CF<sub>3</sub>**: 0.9887; **2-CF<sub>3</sub>**: 0.9884) are close to 1. It indicates that the hole and electron wave functions dominate the description of S<sub>0</sub>–T<sub>1</sub> transition. From Fig. 5, all these studied complexes have similar hole and electron wave functions. The hole wave function is mainly localized in ppy ligand and Ir(III) atom, while the electron wave function is focused on the same ppy ligand. Obviously, the T<sub>1</sub> state of these Ir complexes corresponds to localized transition (LE). In addition, Table 4 shows the distance between centroid of hole and electron (*D*) of **1a**, **1a-Cl**, **1a-F**, **1a-CF<sub>3</sub>**, and **2-CF<sub>3</sub>** are 1.332, 1.513, 1.519, 0.997, 0.822 Å, respectively; therefore, it is expected that these complexes probably have a charge transfer excitation (CT) character. Furthermore, as listed in Table 4, the Ir(III) atom composition from hole to electron of these Ir complexes dramatically decreases (12.17, 11.78, 12.17, 14.16, 23.12, and 19.34 % for **1a**, **1a-Cl**, **1a-F**, **1a-CN**, **1a-CF<sub>3</sub>**, and **2-CF<sub>3</sub>**, respectively), which indicates that the MLCT dominates the description of S<sub>0</sub>–T<sub>1</sub> transition.

### 3.5 The phosphorescence quantum yields

To increase the quantum yield ( $\Phi_{\text{PL}}$ ) from the emissive excited state to the ground state, a large radiative ( $k_r$ ) value and a small nonradiative rate ( $k_{\text{nr}}$ ) are necessary, as shown in the Eq. 1 [26, 27]

$$\Phi_{\text{PL}} = \frac{k_r}{k_r + k_{\text{nr}}} \quad (1)$$

Theoretically, the  $k_r$  is approximated by the Eq. 2. [28–30]

$$k_r = \frac{16\pi^3 10^6 n^3 E_{\text{T1}}^3 \langle \Phi_{\text{S1}} | H_{\text{SOC}} | \Phi_{\text{T1}} \rangle^2 \mu_{\text{S1}}^2}{3h\epsilon_0 \Delta E_{\text{ST}}^2} \quad (2)$$

where  $n$ ,  $h$ ,  $\epsilon_0$  are the refractive index, Planck's constant, and permittivity in vacuum, respectively. The  $E_{\text{T1}}$  is the emitting energy and  $\mu_{\text{S1}}$  denotes transition electric dipole moment in the S<sub>0</sub>–S<sub>1</sub> transition. The  $\langle \Phi_{\text{S1}} | H_{\text{SOC}} | \Phi_{\text{T1}} \rangle$  is SOC matrix element, which is considered as a key factor in determine the  $k_r$  [31]. It is well accepted that the increased

**Table 5** The emission energy of the triplet state ( $E_{T1}$ , eV), metal ligand charge transfer character ( ${}^3\text{MLCT}$ , %), transition electric dipole moment ( $\mu_{S1}$ ,  $D$ ), singlet–triplet splitting energy ( $\Delta E_{S1-T1}$ , eV), as well as  $\Delta\text{dd}_{\text{occ}}$  and  $\Delta\text{dd}^*$  at both the S0 and T1 optimized geometries, along with the experimental radiative ( $k_r$ ,  $10^5 \text{ s}^{-1}$ ) and nonradiative ( $k_{nr}$ ,  $10^5 \text{ s}^{-1}$ ) rate

|                          | $E_{T1}$ (eV)     | ${}^3\text{MLCT}$ (%) | S0                             |                     | T1                             |                     | $\mu_{S1}$ | $\Delta E_{S1-T1}$ (eV) | $k_r$            | $k_{nr}$         |
|--------------------------|-------------------|-----------------------|--------------------------------|---------------------|--------------------------------|---------------------|------------|-------------------------|------------------|------------------|
|                          |                   |                       | $\Delta\text{dd}_{\text{occ}}$ | $\Delta\text{dd}^*$ | $\Delta\text{dd}_{\text{occ}}$ | $\Delta\text{dd}^*$ |            |                         |                  |                  |
| <b>1a</b>                | 2.49              | 16.0                  | 0.39                           | 6.61                | 0.48                           | 6.79                | 1.46       | 0.35                    | 3.4 <sup>b</sup> | 1.6 <sup>b</sup> |
| <b>1a-Cl</b>             | 2.50              | 16.0                  | 0.24                           | 6.21                | 0.30                           | 7.12                | 1.27       | 0.40                    |                  |                  |
| <b>1a-F</b>              | 2.58              | 16.1                  | 0.25                           | 6.73                | 0.29                           | 7.06                | 1.18       | 0.47                    |                  |                  |
| <b>1a-CN</b>             | 2.25              | 18.0                  | 0.12                           | 6.54                | 0.27                           | 7.12                | 1.22       | 0.24                    |                  |                  |
| <b>1a-CF<sub>3</sub></b> | 2.30              | 14.7                  | 0.19                           | 6.82                | 0.38                           | 7.04                | 1.06       | 0.09                    |                  |                  |
| <b>2-CF<sub>3</sub></b>  | 2.24              | 17.2                  | 0.21                           | 6.99                | 0.32                           | 6.98                | 1.13       | 0.18                    |                  |                  |
| <b>1<sup>a</sup></b>     | 2.50 <sup>a</sup> | 13.4 <sup>a</sup>     | 0.29 <sup>a</sup>              | 6.56 <sup>a</sup>   | 0.38 <sup>a</sup>              | 7.05 <sup>a</sup>   | 2.51       | 0.67 <sup>a</sup>       | 2.5 <sup>b</sup> | 2.5 <sup>b</sup> |
| <b>1<sup>a</sup></b>     | 2.50 <sup>a</sup> | 16.2 <sup>a</sup>     | 0.37 <sup>a</sup>              | 6.55 <sup>a</sup>   | 0.49 <sup>a</sup>              | 6.76 <sup>a</sup>   | 1.42       | 0.34 <sup>a</sup>       | 2.6 <sup>b</sup> | 2.3 <sup>b</sup> |

<sup>a</sup> Ref. [16]; <sup>b</sup> Ref. [15]

contribution of  ${}^3\text{MLCT}$  in the T1 state or a minimal  $\Delta E_{ST}$  is beneficial to enhance the SOC and transition probability [32, 33]. Furthermore, the ISC rate can be performed as a function of the energy separation between the singlet S1 and the closest triplet Tn, [34] which means the minimal  $\Delta E_{S1-Tn}$  is beneficial to enhance the ISC rate and thus might increase  $k_r$  [35]. In addition, the  $d$  orbital splittings are usually in determining the phosphorescence efficiency [36, 37]. The  $\Delta\text{dd}_{\text{occ}}$  is the energy differences between the two highest occupied molecular d orbitals, while the  $\Delta\text{dd}^*$  is the splitting between the highest lying occupied and lowest unoccupied d orbitals. Therefore, the calculated  $E_{T1}$ ,  ${}^3\text{MLCT}$ ,  $\mu_{S1}$ ,  $\Delta E_{S1-T1}$ ,  $\Delta\text{dd}_{\text{occ}}$ , and  $\Delta\text{dd}^*$  are collected in Table 5.

As listed in Table 5, the  $E_{T1}$  value of **1a** is similar with that of **1<sup>a</sup>** [16] and **1** [16]; however, the  $k_r$  value of **1a** is obviously different from **1<sup>a</sup>** and **1**, indicating the  $E_{T1}$  value is not a crucial factor to  $k_r$ . Furthermore, it is interesting to find that the participation of  ${}^3\text{MLCT}$  of **1a** (16.0 %) [16] is much larger than that of **1<sup>a</sup>** (13.4 %) [16], and the  $\Delta E_{S1-T1}$  of **1a** (0.35 eV) [16] is much smaller than that of **1<sup>a</sup>** (0.67 eV) [16]; however, their  $k_r$  values are still close to each other. It suggests that other factors may also play an important role in the quantum yield. The larger  $\mu_{S1}$  value of **1<sup>a</sup>** (2.51D) [16] relative to **1a** (1.46D) might be one of the main reasons. In addition, the smaller  $\Delta\text{dd}_{\text{occ}}$  values at both the S0 and T1 states of **1<sup>a</sup>** (0.29 eV for S0 and 0.38 eV for T1) compared with **1a** (0.39 eV for S0 and 0.48 eV for T1) may also result in a larger  $H_{\text{soc}}$  matrix element and a faster the radiative decay rate constant  $k_r$  [37]. Therefore, it can be concluded that the largest  ${}^3\text{MLCT}$  and  $\mu_{S1}$ , as well as the lowest  $\Delta E_{S1-T1}$  and  $\Delta\text{dd}_{\text{occ}}$  values are necessary to judge the  $k_r$ . Furthermore, the excitation energy levels of T2/T3 of designed molecules obtained by M06-2X method based on optimized T2/T3 geometry are shown in Fig. 6. Figure 6 demonstrates that T2 and T3 states of studied complexes are closer to corresponding T1 state; thus, the  $\Delta E_{S1-T1}$  is an important parameter to explain the differences in ISC rate as well as the  $k_r$  values. As shown

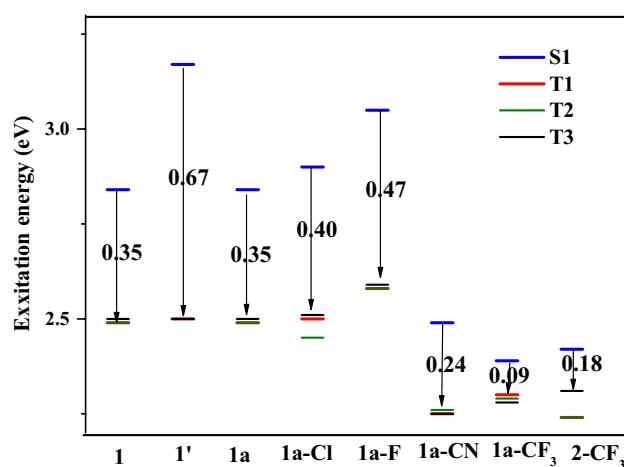


**Fig. 6** The calculated excitation energy levels (eV) of studied complexes

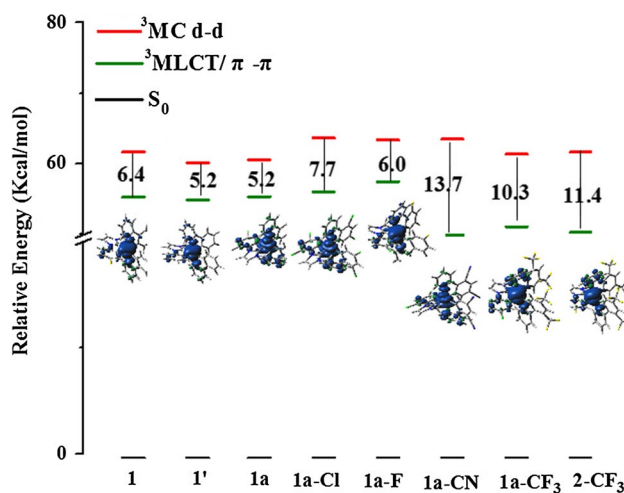


**Fig. 7** The energy level diagram of the theoretical designed and experimental synthesized complexes [15] in the T1 and  ${}^3\text{MC}$  excited states, together with the contour plots of the spin density distribution in the  ${}^3\text{MC}$  state. Complexes **1** [16] and **1<sup>a</sup>** [16] are the synthesized complexes with F substitutions and no substitutions at NHC ligand, respectively



**Table 6** The ionization potential (IP, eV), electron affinities (EA, eV), hole/electron reorganization energy ( $\lambda_h/\lambda_e$ , eV), as well as the energy differences between the hole and electron reorganization energy (eV)

|                          | IP(v) | IP(a) | EA(v) | EA(a) | $\lambda_h$ | $\lambda_e$ | $\Delta\lambda_{h-e}$ |
|--------------------------|-------|-------|-------|-------|-------------|-------------|-----------------------|
| <b>1a</b>                | 6.26  | 6.05  | 0.10  | 0.20  | 0.49        | 0.20        | 0.29                  |
| <b>1a-Cl</b>             | 6.77  | 6.55  | 0.65  | 0.76  | 0.52        | 0.22        | 0.30                  |
| <b>1a-F</b>              | 6.68  | 6.48  | 0.28  | 0.38  | 0.48        | 0.20        | 0.28                  |
| <b>1a-CN</b>             | 7.34  | 7.15  | 1.61  | 1.72  | 0.51        | 0.22        | 0.29                  |
| <b>1a-CF<sub>3</sub></b> | 6.94  | 6.69  | 0.96  | 1.14  | 0.59        | 0.34        | 0.25                  |
| <b>2-CF<sub>3</sub></b>  | 6.87  | 6.64  | 0.89  | 1.07  | 0.57        | 0.35        | 0.22                  |
| <b>1<sup>a</sup></b>     | 6.03  |       | 0.10  |       | 0.52        | 0.01        |                       |
| <b>1<sup>a</sup></b>     | 6.19  |       | 0.01  |       | 0.49        | 0.20        |                       |

<sup>a</sup> Ref. [16]

in Fig. 6, the  $\Delta E_{S_1-T_1}$  is calculated to be 0.24, 0.09, and 0.18 eV for **1a-CN**, **1a-CF<sub>3</sub>**, and **2-CF<sub>3</sub>**, respectively, which is much smaller than experimental synthesized **1'** (0.67 eV) and **1** (0.35 eV). The minimal  $\Delta E_{S_1-T_1}$  will definitely overcome competitive non-radiative decay pathways, therefore, leading to an increased  $k_r$ . Especially for **1a-CF<sub>3</sub>**, its  $\Delta E_{S_1-T_1}$  is close to the most efficient thermally activated delay fluorescence (TADF;  $\Delta E_{S_1-T_1} \leq 0.1$  eV) [38, 39] as reported by Adachi's group. Accordingly, our designed **1a-CF<sub>3</sub>** may have high phosphorescence quantum efficiency. Besides, **1a-CN** has larger <sup>3</sup>MLCT contribution (18 %),  $\mu_{S_1}$  value (1.22D), and smaller  $\Delta\text{dd}_{\text{occ}}$  (at both S0 and T1 state) than **1a-CF<sub>3</sub>** and **2-CF<sub>3</sub>** complexes, suggesting that the introducing CN might increase the possibility of enhancement of  $k_r$  value.

According to Eq. 1, it is necessary to provide some insight into  $k_{nr}$ . The <sup>3</sup>MC  $d-d$  state is considered as one of the most important deactivation pathways for the emission, the separation between the <sup>3</sup>MLCT/ $\pi-\pi$  and <sup>3</sup>MC  $d-d$  states is believed to be closely related to nonradiative pathway [40]. Thus, the energy differences between these states are shown in Fig. 7, along with the spin density of theirs <sup>3</sup>MC  $d-d$  state. As depicted in Fig. 7, the spin density is mainly localized on the Ir atom. The <sup>3</sup>MC  $d-d$  excited state is lying at a relatively higher energy than that of the <sup>3</sup>MLCT/ $\pi-\pi$  excited states, indicating that the emitting phosphors are the most thermodynamically stable ones. The energy difference between the <sup>3</sup>MLCT/ $\pi-\pi$  and <sup>3</sup>MC  $d-d$  state of **1a** is close to that of **1** and **1'**, indicating the nonradiative pathway of **1a** is similar with **1** and **1'**. Thus  $k_r$  of these complex [**1a** ( $1.6 \times 10^5 \text{ s}^{-1}$ ), **1** ( $2.3 \times 10^5 \text{ s}^{-1}$ ), and **1'** ( $2.5 \times 10^5 \text{ s}^{-1}$ )] are close to each other. By introducing these substitutions, **1a-CN** (13.7 kcal/mol), **1a-CF<sub>3</sub>** (10.3 kcal/mol), **2-CF<sub>3</sub>** (11.4 kcal/mol) have larger energy gaps between <sup>3</sup>MLCT/ $\pi-\pi$  and <sup>3</sup>MC  $d-d$  states than experimental synthesized molecules, thus leading to a lower  $k_{nr}$ . Furthermore, the calculated  $\Delta\text{dd}^*$  of **1a-CF<sub>3</sub>**, **1a-CN**, and **2-CF<sub>3</sub>** at their S0 and T1 state have larger value than **1a**, which may result in an effective thermal unaccessible MC and reduce the non-radiative quenching [37].

From the analysis of the participation of <sup>3</sup>MLCT,  $\Delta E_{S_1-T_1}$ ,  $\mu_{S_1}$ ,  $d$  orbital splitting, as well as the energy difference between the <sup>3</sup>MLCT/ $\pi-\pi$  and <sup>3</sup>MC  $d-d$  state, it can be founded that compounds **1a-CN**, **1a-CF<sub>3</sub>** and **2-CF<sub>3</sub>** have relatively larger  $k_r$  values and smaller  $k_{nr}$  values compared with experimental synthesized and other theoretical designed molecules. Thus, **1a-CN**, **1a-CF<sub>3</sub>** and **2-CF<sub>3</sub>** may be potential emitting materials with high efficiency.

### 3.6 Performance of OLEDs

The charge injection, transport, as well as balance are important for the device performances of OLEDs. The ionization potential (IP) and electron affinity (EA) are calculated to evaluate the energy barrier of injection of holes and electrons. A small IP value (large EA) indicates the ease of holes injection (electrons) from the charge injection layer into the emitting materials. The IP and EA are calculated both the vertical excitation (v; at the geometry of neutral molecule) and adiabatic excitation (a: optimized structure for both the neutral and charged molecule). The calculated vertical IP(v), vertical EA(v), adiabatic IP(a), and adiabatic EA(a) of these compounds are listed in Table 6. Table 6 shows both the IP and EA values (both vertical and adiabatic) of **1a** are larger than those of **1'** [16] and **1** [16]. Similarly, **1a-CF<sub>3</sub>** gives much larger EAs compared with **2-CF<sub>3</sub>**. Clearly the electron injection ability of this type of complex can be enhanced by introducing Cl atoms at NHC ligand instead of F atoms, which is consistent with the analyses in their LUMO energies. In addition, it can be seen that the calculated IP values (both vertical and adiabatic) decrease in the order: **1a-CN** > **1a-CF<sub>3</sub>** > **2-CF<sub>3</sub>** > **1a-Cl** > **1a-F** > **1a**, suggesting the ability of hole injection gradually increases. This tendency is consistent with the trend of HOMO energies in Sect. 3.2. For EA values (both vertical and adiabatic), the introduction of CN, CF<sub>3</sub>, Cl, and F has a positive influence on increasing the EA values. The calculated EA values (both vertical and adiabatic) decrease in the following order: **1a-CN** > **1a-CF<sub>3</sub>** > **2-CF<sub>3</sub>** > **1a-Cl** > **1a-F** > **1a**, indicating that these designed complexes

accept an electron more easily than **1a**. This trend is well consistent with the order of the LUMO energy.

The mobility of the hole and electron is investigated based on the Marcus theory [41]. As well known, for efficient charge transport, the reorganization energy is required to be small. The hole/electron reorganization energy ( $\lambda_h/\lambda_e$ ) is calculated as described in previous work [42], and the calculated values of  $\lambda_h$  and  $\lambda_e$  are also listed in Table 5. From the calculated data in Table 5, **1a** has smaller  $\lambda_e$  (0.20 eV) than its  $\lambda_h$  (0.49 eV). It means that **1a** is an excellent electron transport material, which is similar with its derivatives **1'** [16] and **1** [16]. After introducing the electron-withdrawing (F, Cl, and CN) substitutions at ppy ligands, **1a-F**, **1a-Cl**, and **1a-CN** have similar  $\lambda_e$  and  $\lambda_h$  values with those of **1a**. Their  $\lambda_h$  values are almost two times larger than theirs  $\lambda_e$  values, suggesting that **1a-Cl**, **1a-F**, and **1a-CN** still have excellent electron transport ability. With respect to **1a-CF<sub>3</sub>** and **2-CF<sub>3</sub>**, the  $\lambda_e$  and  $\lambda_h$  values become larger, indicating that they have relatively poor charge transport rate comparison with those of **1a**. It is also found that the energy differences between  $\lambda_e$  and  $\lambda_h$  ( $\Delta\lambda_{h-e}$ ) for all these designed complexes are ca. 0.30 eV, implying that these materials are not suitable to be used as emitting-layer materials in OLEDs because of their unbalanced hole and electron transport.

## 4 Conclusion

We have employed DFT and TDDFT investigations on the electronic structures, photophysical properties, and phosphorescence quantum yields of a series of Ir complexes coordinated with 2-phenylpyridine (ppy) and N-heterocyclic carbenes (NHC) ligands. It is found that the introduction of F, Cl, CN, and CF<sub>3</sub> substitutions on the ppy ligands can strengthen the metal–ligand bond, stabilize the LUMO energy levels, as well as increase the absorption intensities and participations of MLCT in the absorption band. Through the analyses of participation of <sup>3</sup>MLCT,  $\Delta E_{S_1-T_1}$ ,  $\mu_{S_1}$ ,  $d$  orbital splitting, as well as the energy difference between the <sup>3</sup>MLCT/ $\pi$ - $\pi$  and <sup>3</sup>MC  $d$ - $d$  state, it can be inferred that compounds **1a-CN**, **1a-CF<sub>3</sub>**, and **2-CF<sub>3</sub>** have larger  $k_r$  values and smaller  $k_{nr}$  values compared with other molecules. In addition, these designed complexes are suitable to be used as electron transport materials because of better electron injection and transfer rates. These structure–property relationships are hoped to provide valuable information to obtain highly efficient phosphorescent emitters.

**Acknowledgments** Financial supports from NSFC (Nos. 21243006 and 51304193), the Basic Research Program of Jiangsu Province (No. BK20130172), the Fundamental Research Funds for the Central

Universities (No. 2013QNA14). A Project Funded by the Priority Academic Program Development of Jiangsu Higher Education Institutions. We are grateful to the High Performance Computing Center of China University of Mining and Technology for the award of CPU hours to accomplish this work.

## References

- Lamansky S, Djurovich P, Murphy D, Abdel-Razzaq F, Lee HE, Adachi C, Burrows PE, Forrest SR, Thompson ME (2001) *J Am Chem Soc* 123:4304–4312
- Zhou G, Wong W-Y, Yao B, Xie Z, Wang L (2007) *Angew Chem Int Ed* 46:1149–1151
- Zhao YY, Gao HF, Wang XM, Qi HL (2015) *Inorg Chem* 54:1446–1453
- Hofbeck T, Yersin H (2010) *Inorg Chem* 49:9290–9299
- Kim DH, Cho NS, Oh HY, Yang JH, Jeon WS, Park JS, Suh MC, Kwon JH (2011) *Adv Mater* 23:2721–2726
- Tian N, Aulin YV, Lenkeit D, Pelz S, Mikhnenko OV, Blom PWM, Loi MA, Holder E (2010) *Dalton Trans* 39:8613–8615
- Finkenzeller WJ, Yersin H (2003) *Chem Phys Lett* 377:299–305
- Baldo MA, Lamansky S, Burrows PE, Thompson ME, Forrest SR (1999) *Appl Phys Lett* 75:4–6
- Sajoto T, Djurovich PI, Tamayo A, Yousufuddin M, Bau R, Thompson ME, Holmes RJ, Forrest SR (2005) *Inorg Chem* 44:7992–8003
- Wu Y, Wu SX, Li HB, Geng Y, Su ZM (2011) *Dalton Trans* 40:4480–4488
- Ma MS, Zou LY, Li Y, Ren AM, Feng JK (2015) *Org Electron* 22:180–190
- Ren XF, Kang G-J, Zhang S-F, Ren A-M, Wong W-Y, Zhou GJ, Liu Y-L (2015) *J Photochem Photobiol A Chem* 311:85–94
- Deaton JC, Young RH, Lenhard JR, Rajeswaran M, Huo S (2010) *Inorg Chem* 49:9151–9161
- Wang L, Wu Y, Geng Y, Wu J, Zhu DX, Su ZM (2014) *J Phys Chem A* 118:5058–5067
- Stringer BD, Quan LM, Barnard PJ, Wilson DJD, Hogan CF (2014) *Organometallics* 33:4860–4872
- Kang GJ, Ren XF, Bai SY (2015) *J Organomet Chem* 785:44–51
- Adamo C, Barone V (1998) *J Chem Phys* 108:664–675
- Hay PJ, Wadt WR (1985) *J Chem Phys* 82:270–283
- Wadt WR, Hay PJ (1985) *J Chem Phys* 82:284–298
- Hay PJ, Wadt WR (1985) *J Chem Phys* 82:299–310
- Lu T, Chen FW (2012) Multiwfn: a multifunctional wavefunction analyzer. *J Compd Chem* 33:580–592
- Zhao Y, Truhlar DG (2008) *J Theor Chem Acc* 120:215–241
- Bark T, Thummel RP (2005) *Inorg Chem* 44:8733–8739
- Martin RL (2003) *J Chem Phys* 118:4775–4777
- Frisch MJ, Trucks GW, Schlegel HB, Scuseria GE, Robb MA, Cheeseman JR, Scalmani G, Barone V, Mennucci B, Petersson GA, Nakatsuji H, Caricato M, Li X, Hratchian HP, Izmaylov AF, Bloino J, Zheng G, Sonnenberg JL, Hada M, Ehara M, Toyota K, Fukuda R, Hasegawa J, Ishida M, Nakajima T, Honda Y, Kitao O, Nakai H, Vreven T, Montgomery JA Jr, Peralta JE, Ogliaro F, Bearpark M, Heyd JJ, Brothers E, Kudin KN, Staroverov VN, Kobayashi R, Normand J, Raghavachari K, Rendell A, Burant JC, Iyengar SS, Tomasi J, Cossi M, Rega N, Millam JM, Klene M, Knox JE, Cross JB, Bakken V, Adamo C, Jaramillo J, Gomperts R, Stratmann RE, Yazyev O, Austin AJ, Cammi R, Pomelli C, Ochterski JW, Martin RL, Morokuma K, Zakrzewski VG, Voth GA, Salvador P, Dannenberg JJ, Dapprich S, Daniels AD, Farkas O, Foresman JB, Ortiz JV, Cioslowski J, Fox DJ (2009) *Gaussian 09, Revision B.04*. Gaussian, Inc, Wallingford
- You Y, Park SY (2009) *Dalton Trans* 8:1267–1282

27. Siddique ZA, Yamanoto Y, Ohno T, Nozaki K (2003) *Inorg Chem* 42:6366–6378
28. Turro N (1991) *Modern molecular photochemistry*. University Science Books, Palo Alto
29. Haneder S, Como ED, Feldmann J, Lupton JM, Lennartz C, Erk P, Fuchs E, Molt O, Münster I, Schildknecht C, Wagenblast G (2008) *Adv Mater* 20:3325–3330
30. Minaev B, Baryshnikov G, Agren H (2014) *Phys Chem Chem Phys* 16:1719–1758
31. Si YL, Sun XB, Liu YQ, Qu XC, Wang Y, Wu ZJ (2014) *Dalton Trans* 43:714–721
32. Sprouse S, King KA, Spellane PJ, Watts RJ (1984) *J Am Chem Soc* 106:6647–6653
33. Shang XH, Han DM, Zhan Q, Zhang G, Li DF (2014) *Organometallics* 33:3300–3308
34. Kozhevnikov DN, Kozhevnikov VN, Shafikov MZ, Prokhorov AM, Bruce DW, Gareth JA (2011) *Williams. Inorg Chem* 50:3804–3815
35. Burin AL, Ratner MA (1998) *J. Chem. Phys.* 109:6092–6102
36. Yersin H, Finkenzeller WJ (2008) In: Yersin H (ed) *Highly efficient OLEDs with phosphorescent materials*. Wiley-VCH, Weinheim, pp 1–97
37. Tong GSM, Che CM (2009) *Chem Eur J* 15:7225–7237
38. Uoyamal H, Goushi K, Shizu K, Nomura H, Adachi C (2012) *Nature* 492:234–238
39. Nakanotani H, Higuchi T, Furukawa T, Morimoto K, Numata M, Tanaka H, Sagara Y, Yasuda T, Adachi C (2014) *Nat Commun* 5:4016–4023
40. Alary F, Heully JL, Bijeire L, Vicendo P (2007) *Inorg Chem* 46:3154–3165
41. Marcus RA (1993) *Rev Mod Phys* 65:599–610
42. Ren XF, Ren AM, Feng JK, Sun CC (2009) *J Photochem Photobiol A Chem* 203:92–99